Modeling colloid and microorganism transport and release with transients in solution ionic strength

Scott A. Bradford,[1] Saeed Torkzaban,[2] Hyunjung Kim,[3] and Jiri Simunek[4]

Received 30 May 2012; revised 17 July 2012; accepted 20 July 2012; published 7 September 2012.

[1] The transport and fate of colloids, microorganisms, and nanoparticles in subsurface environments is strongly influenced by transients in solution ionic strength (IS). A sophisticated dual-permeability transport model was modified and a theory was developed to mechanistically account for the transport, retention, and release of colloids with transients in IS. In particular, colloid release in the model was directly related to the balance of applied hydrodynamic and resisting adhesive torques that determined the fraction of the solid surface area that contributed to colloid immobilization (S_f). The colloid sticking efficiency (α) and S_f were explicit functions of IS that determined the rates of colloid interaction with the solid, immobilization on the solid, colloid release from the solid and back into the bulk aqueous phase, and the maximum amount of colloid retention. The developed model was used to analyze experimental transport and release data with transients in IS for 1.1 and 0.11 μm latex microspheres, *E. coli* D21g, and coliphage ϕX174. Comparison of experimental values of S_f(IS) with predictions based on mean interaction energies indicated that predictions needed to account for the influence of physical and/or chemical heterogeneity on colloid immobilization. This was especially true for smaller colloids because they were more sensitive to microscopic heterogeneities that produced mainly irreversible interaction in a primary minimum and greater hysteresis in S_f(IS) with IS. Significant deviations between experimental and predicted values of α(IS) were observed for larger colloids when hydrodynamic forces were not accounted for in the predictions. A sensitivity analysis indicated that colloid release with IS transients was not diffusion controlled, but rather occurred rapidly and with low levels of dispersion. The calibrated model provided a satisfactory description of the observed release behavior for a range of colloid types and sizes and a general theoretical foundation to develop predictions for the influence of solution chemistry on the transport, retention, and release of colloids.

Citation: Bradford, S. A., S. Torkzaban, H. Kim, and J. Simunek (2012), Modeling colloid and microorganism transport and release with transients in solution ionic strength, *Water Resour. Res.*, *48*, W09509, doi:10.1029/2012WR012468.

1. Introduction

[2] Release of colloids from soils may occur as a result of diffusion [*Ryan and Gschwend*, 1994; *Simoni et al.*, 1998; *Dong et al.*, 2002; *Shen et al.*, 2007], an increase in hydrodynamic forces [*Hubbe*, 1984; *Sharma et al.*, 1992; *Torkzaban et al.*, 2007; *Bradford et al.*, 2011a], and a reduction in adhesive forces [*Ryan and Gschwend*, 1994; *Bergendahl and Grasso*, 1999; *Lenhart and Saiers*, 2003; *Torkzaban et al.*, 2010]. The detachment coefficient is frequently considered to be a diffusion controlled process that is a function of the diffusion coefficient and the boundary layer thickness [*Ryan and Gschwend*, 1994; *Ryan and Elimelech*, 1996]. However, this approach does not account for the strength of the adhesive interaction and the removal of colloids due to hydrodynamic mechanisms such as rolling, lifting, or sliding [*Bergendahl and Grasso*, 1998, 1999; *Tsai et al.*, 1991]. A constant value of the colloid detachment coefficient is therefore unlikely to account for temporal changes in colloid release that will commonly occur as a result of transients in solution chemistry and flow rate during infiltration and recharge events, freshwater intrusion, dilution of contaminant plumes, and near injection and extraction wells.

[3] It is well accepted that changes in solution chemistry (IS, pH, cation exchange, and concentration of organic matter) will impact the electric double layer thickness and/or the zeta potential and thereby alter electrostatic interactions [*Ryan and Elimelech*, 1996; *Grolimund and Borkovec*, 2006]. Chemical perturbations are often used to create interaction energies between colloids and surfaces in order to induce particle attachment [*Goldshmid et al.*, 1973; *Nocito-Gobel and*

[1]U.S. Salinity Laboratory, ARS, USDA, Riverside, California, USA.
[2]CSIRO Land and Water, Glen Osmond, South Australia, Australia.
[3]Department of Mineral Resources and Energy Engineering, Chonbuk National University, Jeonju, South Korea.
[4]Department of Environmental Sciences, University of California, Riverside, California, USA.

Corresponding author: S. A. Bradford, U.S. Salinity Laboratory, ARS, USDA, 450 West Big Springs Rd., Riverside, CA 92507, USA. (scott.bradford@ars.usda.gov)

0043-1397/12/2012WR012468

Tobiason, 1996; *Shiratori et al.*, 2007; *Tosco et al.*, 2009] or detachment [*Bales et al.*, 1991; *McDowell-Boyer*, 1992; *Ryan and Gschwend*, 1994; *Nocito-Gobel and Tobiason*, 1996; *Roy and Dzombak*, 1996; *Grolimund et al.*, 2001; *Lenhart and Saiers*, 2003; *Shiratori et al.*, 2007; *Tosco et al.*, 2009; *Bradford and Kim*, 2010]. *Ryan and Gschwend* [1994] reported that changes in solution chemistry must be great enough to eliminate the energy barrier in order to successfully achieve detachment. A critical salt concentration has been reported for particle release [*Khilar and Fogler*, 1984; *Lenhart and Saiers*, 2003]. *Tosco et al.* [2009] reported that chemical perturbations that induced detachment were well correlated with the disappearance of secondary minima under unfavorable attachment conditions.

[4] Hysteresis in the amount of colloid/microbe retention and release has been observed with changes in the IS of the eluting solution [*Torkzaban et al.*, 2010; *Bradford and Kim*, 2012]. Consideration of mean adhesive interactions cannot explain this behavior [*Bradford and Kim*, 2012]. *Bradford and Kim* [2012] found that hysteresis occurred because retention and release were dependent on the relative size of the colloids/microbes to microscale chemical (metal oxides) or physical (surface roughness) heterogeneity, the Debye length, and spatial variations in the applied hydrodynamic torque. A larger number of colloids interacted with these heterogeneities at thinner (higher IS) than a thicker (lower IS) double layer as they move near the solid surface and find a local minimum in the interaction energy. It is therefore more difficult to remove colloids from local minima found under higher than lower IS conditions by changing the IS. Colloids tended to be reversibly retained in sand with transients in IS when they were larger than the heterogeneity, whereas they were mainly irreversibly retained when they were similar in size to the heterogeneity. This occurs because the zone of electrostatic influence and the applied hydrodynamic torque are functions of the particle size [*Torkzaban et al.*, 2007; *Duffadar and Davis*, 2008].

[5] Several models have been proposed to simulate colloid release with transients in solution IS [*Lenhart and Saiers*, 2003; *Grolimund and Borkovec*, 2006; *Tosco et al.*, 2009]. *Lenhart and Saiers* [2003] considered heterogeneity in the interaction energy of the colloid populations by dividing attached colloids into a series of compartments, each with a characteristic critical salt concentration for release. Similarly, *Grolimund and Borkovec* [2006] divided particles into discrete populations. However, in their model a single attachment coefficient was employed for all populations, whereas separate detachment coefficients were used for each population. *Tosco et al.* [2009] simulated the release of colloids during transient IS conditions using a two-site kinetic attachment and detachment model. The models of *Lenhart and Saiers* [2003] and *Tosco et al.* [2009] also included terms for blocking, whereas the model of *Grolimund and Borkovec* [2006] included an empirical term in the attachment and detachment coefficients that accounted for the fraction of exchange sites occupied by divalent cations. All of the above models employ attachment and detachment coefficients that were empirical functions of IS. Determination of these functions required extensive optimization to experimental data to achieve satisfactory descriptions, and true predictions were not possible.

[6] *Bradford et al.* [2011b] developed a mathematical model to mechanistically account for colloid transport in the bulk aqueous phase and adjacent to the solid surface, and rates of colloid collision, interaction, release and immobilization on the solid phase. This model is capable of simulating exponential, hyperexponential, uniform, and nonmonotonic retention profiles. The objective of this work is to improve our ability to simulate colloid transport, retention, and release with transients in solution IS by extending this model. Continuum-scale parameters were developed for the model to account for the influence of diffusion, adhesion, and hydrodynamic forces and/or torques on colloid retention and release with variations in IS. This general modeling framework was subsequently used to analyze experimental transport and release data with transients in IS for two sized latex microspheres, *E. coli* D21g, and coliphage φX174. This model and analyses improves our understanding of the hysteretic dependence of the adhesive interactions on solution IS and velocity, and the rates of colloid release and dispersion.

2. Experimental Information

[7] *Bradford and Kim* [2012] presented experimental deposition and release data with transients in IS for fluorescent 1.1 and 0.11 μm carboxyl modified latex (CML) microspheres, *E. coli* D21g, and coliphage φX174. Experimental details are given in this publication, but will be briefly highlighted below. Ottawa sand that is 360 μm in size was cleaned using a salt cleaning method [*Bradford and Kim*, 2010] to remove trace amounts of clay. The sand was then wet packed to a porosity of 0.32 to 0.36 in 4.8 cm diameter by 15 cm long columns that were equipped with an adjustable fitting at the top so that different column lengths were possible. Various NaCl solutions at selected IS (6, 31, 56, and 106 mM) and buffered to pH = 10 were prepared for the resident, tracer, and eluting solutions. This pH = 10 was selected to maximize the potential for colloid/microbe release with transients in solution IS. It should be mentioned that colloid/microbe release is expected to be diminished at lower pH values, and will be completely eliminated under favorable attachment conditions.

[8] The sand in the columns was equilibrated by flushing the column with several pore volumes (PVs) of resident solution at a given solution IS, leaving this solution in the column over overnight, and then flushing several additional PVs of resident solution through the column. A tracer solution of microspheres, *E. coli* D21g, or φX174 was pumped through the packed columns at a steady Darcy velocity of 0.09 to 0.12 cm min^{-1} for several pore volumes (phase 1) followed by continued flushing with the eluting solution at the same velocity and IS (phase 2). The influent IS was subsequently lowered in several steps to study mobilization/release (phase 3). After changing the IS in each step, the column was flushed with the lowered solution IS until the change in effluent concentration was minimal. The concentrations of fluorescent microspheres, *E. coli* D21g, and φX174 were determined in the column effluent using a fluorometer, a spectrophotometer, and the double agar overlay method, respectively. A mass balance was conducted based on measured concentrations in the influent and effluent.

[9] The zeta potentials for the CML microspheres, *E. coli* D21g, φX174, and Ottawa sand in the various solution chemistries were measured and sphere-plate interaction energies were subsequently calculated using DLVO theory [*Derjaguin and Landau*, 1941; *Verwey and Overbeek*,

1948]. It should be mentioned that mean zeta potentials and calculated interaction energies do not account for the influence of microscopic physical and chemical heterogeneity on colloid adhesive parameters [*Foppen and Schijven*, 2006; *Duffadar and Davis*, 2007, 2008; *Kim et al.*, 2008; *Metge et al.*, 2010]. *Bradford and Kim* [2012] reported that the salt treated sand exhibited significant amounts of heterogeneity. For example, the sand surface roughness was visualized using a scanning electron microscopy and found to have a large influence on the measured surface area (a BET surface area of 560 $cm^2\ g^{-1}$ compared to a geometric value of around 64 $cm^2\ g^{-1}$). To determine the influence of chemical heterogeneity the sand was stored in 12 N HCl acid overnight and 12.3 μg of Fe per gram of sand was measured in the acid rinse. It should be mentioned that *E. coli* D21 g is a mutant with minimal amounts of lipopolysaccharides [*Gmeiner and Schlecht*, 1980; *Walker et al.*, 2004]. The influence of surface macromolecules on calculated interaction energies is therefore expected to be minimal for *E. coli* D21 g.

3. Mathematical Model

[10] Our conceptual model for colloid transport, retention, and release in porous media assumes that the pore space is divided into two mobile regions, a higher-velocity region 1 in the bulk solution and a low-velocity region 2 adjacent to the solid surface. The rate of colloid exchange between regions 1 and 2 is quantified using first-order kinetic expressions. The fraction of the colloids in region 2 that interacts with the solid phase at any given time is a function of IS, and this fraction is subject to kinetic retention and release that also depends on the solution chemistry. Immobilized colloids on the solid phase may fill up retention locations over time or a fraction may be released into region 2 with transients in solution IS or velocity. Corresponding mathematical expressions for this conceptual model are provided below.

[11] We assume that colloid transport and retention is a function of IS that varies with distance and time. The IS of a 1:1 electrolyte can easily be determined from the solution of the mass balance equation for a conservative tracer (e.g., chloride ion) throughout the entire pore space (sum of regions 1 and 2) as

$$\frac{\partial(\theta_{wt}C_{is})}{\partial t} = -\frac{\partial J_{is}}{\partial z} \tag{1}$$

where θ_{wt} (dimensionless) is the volumetric water content, t [T; T denotes units of time] is time, and z [L; L denotes units of length] is the depth, C_{is} [$M_{is}\ L^{-3}$; M_{is} denotes the tracer mass] is the tracer concentration (equal to the IS for a 1:1 electrolyte) in the aqueous phase, and J_{is} [$M_{is}\ L^{-2}\ T^{-1}$] is the tracer flux.

[12] The colloid mass balance equations for regions 1 (bulk fluid), 2 (adjacent to the solid phase), and the solid are given as

$$\frac{\partial(\theta_{w1}C_1)}{\partial t} = -\frac{\partial J_1}{\partial z} - \theta_{w1}\alpha k_{12}C_1 + \theta_{w2}(1-\alpha)k_{21}C_2 \tag{2}$$

$$\frac{\partial(\theta_{w2}C_2)}{\partial t} = -\frac{\partial J_2}{\partial z} + \theta_{w1}\alpha k_{12}C_1 - \theta_{w2}(1-\alpha)k_{21}C_2 - \theta_{w2}\psi_{2s}k_{2s}C_2 + \rho_b k_d(s - f_c s_i) \tag{3}$$

$$\frac{\partial(\rho_b s)}{\partial t} = \theta_{w2}\psi_{2s}k_{2s}C_2 - \rho_b k_d(s - f_c s_i) \tag{4}$$

where subscripts 1 and 2 denote the respective regions, C [$N_c\ L^{-3}$; N_c denotes the number of colloids] is the colloid concentration in the aqueous phase, J [$N_c L^{-2} T^{-1}$] is the colloid flux (sum of the advective and dispersive flux), s [$N_c\ M^{-1}$; M denotes units of mass of soil] is the colloid concentration on the solid phase, s_i [$N_c\ M^{-1}$] is the value of s at the end of the deposition phase 1 and before a reduction in IS, f_c (dimensionless) is the fraction of colloids on the solid phase that still remain immobilized after a reduction in IS, k_d [T^{-1}] is the colloid detachment rate coefficient from the solid phase to region 2, k_{2s} [T^{-1}] is the colloid immobilization rate coefficient from region 2 to the solid phase, k_{12} [T^{-1}] is the mass transfer coefficient for colloids from region 1 to 2, k_{21} [T^{-1}] is the mass transfer coefficient for colloids from region 2 to 1, α (dimensionless) is the colloid sticking efficiency, and ρ_b [$M\ L^{-3}$] is the bulk density. The parameter ψ_{2s} (dimensionless) accounts for time and concentration dependent blocking using a Langmuirian approach as [*Adamczyk et al.*, 1994]

$$\psi_{2s} = 1 - \frac{s}{s_{\max}} \tag{5}$$

where $s_{\max}$ [$N_c\ M^{-1}$] is the maximum solid phase concentration of retained colloids. The total water flux (q_t; LT^{-1}), volumetric water content, and flux concentration of colloids (C_t, $N_c\ L^{-3}$) are given in the model as

$$q_t = q_1 + q_2 \tag{6}$$

$$\theta_{wt} = \theta_{w1} + \theta_{w2} \tag{7}$$

$$C_t = \frac{q_1 C_1 + q_2 C_2}{q_1 + q_2} \tag{8}$$

where q_1 and q_2 [LT^{-1}] are the Darcy velocities for regions 1 and 2, respectively.

[13] Equations (2)–(8) are similar to that presented by *Bradford et al.* [2011b], but now colloid transport and retention parameters are functions of C_{is} and a detachment term has been added from the solid phase to region 2. For a given time step, equation (1) is solved first for the solution IS, then the colloid transport parameters are updated, and finally equations (2)–(5) are solved for the colloid concentrations. Determination of the model parameters and the coupling with C_{is} will be described in detail in the next section.

[14] The model outlined above has been implemented into the COMSOL software package (COMSOL, Inc., Palo Alto, California). For the simulations discussed below, a third-type boundary condition was used at the inlet, and a concentration gradient of zero was fixed at z equal to the outlet depth. The simulation domain was selected to be consistent

with the packed column lengths (L_c, L), and the initial concentration in the simulation domain was zero.

4. Model Parameters

[15] *Bradford et al.* [2011b] described in detail methods to estimate the above model parameters. In brief, $q_2 = v_2\theta_{w2}$ and $\theta_{w2} = A_sL_2$, where v_2 (L T^{-1}) is the median water velocity in region 2 which occurs at a distance of 0.5 L_2 from the solid-water interface (SWI), $L_2 = 2r_c + h$ is the boundary thickness (L), r_c (L) is the particle radius, h (L) is the separation distance, and A_s (L^{-1}) is the geometric surface area of the porous medium per unit volume. Pore-scale simulations of water flow in sphere packs were used to determine the cumulative density function (CDF) of water velocities in region 2 [*Bradford et al.*, 2011a]. This information was further extended by these authors using scaling and interpolation techniques to predict v_2 for a range of grain sizes and distributions, water velocities, and particle sizes. Information on q_2 and θ_{w2} was used in conjunction with equations (6) and (7) to determine q_1 and θ_{w1}, respectively. Values of the hydrodynamic dispersion coefficients in regions 1 and 2 were set equal to the product of their respective pore water velocity and a constant dispersivity (λ, L). The value of k_{12} was predicted using filtration theory [*Yao et al.*, 1971] and a published correlation for the collector efficiency [*Tufenkji and Elimelech*, 2004]. The value of k_{21} was set equal to k_{12} to be consistent with reported values in the literature [*Gargiulo et al.*, 2007, 2008; *Wang et al.*, 2011] and linear equilibrium sorption with the retardation coefficient (R) equal to $R = 1 + \alpha/(1 - \alpha)$.

[16] The model parameters α, s_{max}, k_{2s}, ψ_{2s}, f_c, and k_d are all functions of the adhesive interaction energy between the colloid and the solid surface (Φ_{min}) which varies with C_{is}. When mean zeta potentials are used in DLVO calculations [*Derjaguin and Landau*, 1941; *Verwey and Overbeek*, 1948] the value of Φ_{min} equals the depth of the secondary minimum under unfavorable attachment conditions. The relationship between these parameters and Φ_{min} will first be discussed before we address the determination of $\Phi_{min}(C_{is})$.

[17] The kinetic energy method [*Simoni et al.*, 1998; *Dong et al.*, 2002; *Shen et al.*, 2007] is used herein to provide a preliminary estimate for α as

$$\alpha = \mathrm{erf}\left(\sqrt{\Phi_{min}}\right) - \sqrt{\frac{4\Phi_{min}}{\pi}}\exp(-\Phi_{min}) \tag{9}$$

This approach assumes that the amount of colloids that interact with the solid surface in region 2 is only dependent on the kinetic energy of diffusing colloids and the strength of the mean adhesive interaction energy.

[18] The value of s_{max} for a given value of C_{is} can be estimated as [*Kim et al.*, 2009; *Bradford et al.*, 2009]:

$$s_{max} = \frac{(1-\gamma)A_sS_f}{A_c\rho_b} \tag{10}$$

where A_c [L^2 N^{-1}] is the cross section area per colloid, A_s [L^{-1}] is the solid surface area per unit volume, S_f (dimensionless) is the fraction of the surface area that is favorable for colloid retention, and γ (dimensionless) is the porosity of a monolayer packing of colloids on the solid surface. In this work we assume a value of $\gamma = 0.5$ in all simulations based on information presented by *Johnson and Elimelech* [1995].

[19] *Bradford et al.* [2011a] presented a detailed approach to predict the value of S_f based on the balance of applied hydrodynamic ($T_{applied}$, ML^2T^{-2}) and resisting adhesive ($T_{adhesion}$, ML^2T^{-2}) torques. In summary, pore-scale simulations and scaling approaches were used to determine the lognormal CDF of $T_{applied}$ on packs of smooth, spherical collectors for different velocities, collector sizes and colloid sizes. The CDF of $T_{applied}$ is subsequently evaluated at $T_{adhesion}$ to determine S_f as

$$S_f = \frac{1}{2} + \frac{1}{2}erf\left(\frac{\ln(T_{adhesion}) - \mu}{\sigma\sqrt{2}}\right) \tag{11}$$

where μ and σ are the mean and variance of the lognormal CDF of $T_{applied}$. The value of μ for the lognormal distribution is defined as

$$\mu = \ln(T_{50}) \tag{12}$$

The value of T_{50} [ML^2T^{-2}] corresponds to the median value of $T_{applied}$ on the SWI.

[20] The value of $T_{adhesion}$ in equation (11) is equal to the product of a lever arm (l_x, L) and the pull-off adhesive force (F_A, M L T^{-2}) that is required to mobilize a colloid from Φ_{min} [*Bergendahl and Grasso*, 1998]. The value of F_A may be estimated using the Derjaguin and Langbein approximations as $\Phi_{min}(C_{is})/h$ [*Israelachvili*, 1992; *Bergendahl and Grasso*, 2000]. Only a portion of the colloid's projection on the SWI makes a meaningful contribution to F_A and this is referred to as the zone of electrostatic influence [*Duffadar and Davis*, 2008]. A value of l_x occurs within the zone of electrostatic influence due to colloid deformation [*Bergendahl and Grasso*, 1998] and/or friction arising from surface roughness and/or chemical heterogeneity [*Duffadar and Davis*, 2008]. Some researchers have assumed an empirical value of l_x to account for friction [*Duffadar and Davis*, 2008]. Alternatively, theory by Johnson, Kendall, and Roberts (JKR) may be used to estimate l_x as a result of resistance due to deformation at separation [*Johnson et al.*, 1971; *Maugis*, 1992] for colloid attachment under favorable or unfavorable conditions [*Bergendahl and Grasso*, 2000; *Li et al.*, 2005; *Bradford et al.*, 2007, 2011a; *Torkzaban et al.*, 2007, 2008; *Shen et al.*, 2010]. It should be mentioned that Derjaguin-Muller-Toporov developed an alternative model (the DMT model) to determine l_x as a result of deformation [*Derjaguin et al.*, 1975]. In contrast to the JKR model, the DMT model predicts that the $l_x = 0$ at separation. No colloid immobilization occurs in the presence of fluid flow when $l_x = 0$ because F_A is perpendicular to the fluid drag force. This result is not consistent with many experimental observations summarized by *Torkzaban et al.* [2009, 2010]; e.g., microscopic observations of colloid immobilization, significant amounts of colloid retention under unfavorable attachment conditions, and abrupt colloid release with changes in the solution chemistry. We have therefore chosen to use l_x at separation from the JKR model.

[21] The parameter S_f is not only an important parameter for determining s_{max} and ψ_{2s} according to equations (10) and (5), respectively, it also is strongly related to k_{2s}, f_c, and k_d as will be discussed below. *Bradford et al.* [2011b] estimated k_{2s} from the median time it takes a colloid in

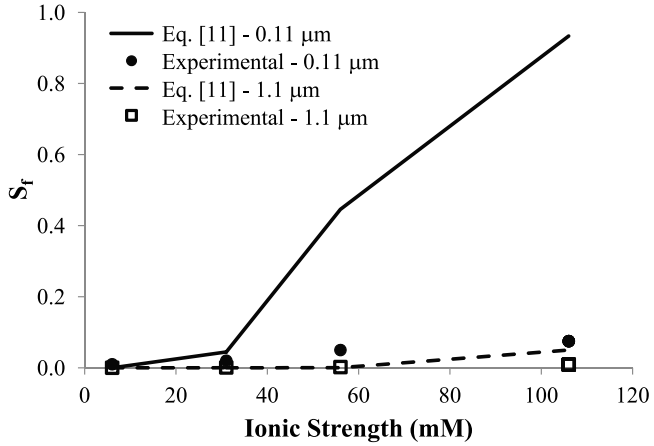

Figure 1. Experimental and predicted values of S_f as a function of IS for 0.11 and 1.1 μm CML microspheres. Experimental values of S_f were obtained by optimization of the simulated and measured breakthrough curves during phases 1 and 2. The predicted values of S_f were obtained using equations (11) and (12) in conjunction with reported values of Φ_{min} [*Bradford and Kim*, 2012] and JKR theory [*Johnson et al.*, 1971] to determine $T_{adhesion}$.

region 2 to move to a location where the torque balance is favorable for retention:

$$k_{2s} = \frac{2N_f v_2}{\pi d_{50}(1 - S_f)} \tag{13}$$

where N_f (dimensionless) is the number of favorable locations of equal size and distribution on the collector surface and d_{50} [L] is the median grain size. On a smooth, chemically homogeneous collector the value of N_f may reflect the average number of grain-grain contacts; e.g., N_f = 5. Alternatively, if surface roughness or chemical heterogeneity is controlling the value of S_f then N_f is given as

$$N_f = \frac{\pi d_{50} S_f}{2 d_f} \tag{14}$$

Here d_f [L] is equal to the average size of the heterogeneity parallel to the collector surface.

[22] The amount of colloids that are released with transients in IS is directly related to changes in the balance of $T_{applied}$ and $T_{adhesion}$. The value of f_c is therefore directly related to S_f as

$$f_c = \frac{S_f}{S_{if}} \tag{15}$$

where S_{if} (dimensionless) is the value of S_f before the reduction in IS. The value of k_d is determined by the rate of change in adhesive force and/or torque with changes in IS. This should theoretically be a very rapid response, as has been confirmed by *Lenhart and Saiers* [2003]. In this work, we initially estimate k_d as

$$k_d = k_{21} H_o(s - f_c s_i) \tag{16}$$

where $H_o(s - f_c s_i)$ is the Heaviside function that is equal to 1 when $s > f_c s_i$ and 0 when $s \le f_c s_i$. Note that the value of $s > f_c s_i$ can occur when f_c changes with S_f (which is a function of $\Phi_{min}(C_{is})$). In the absence of additional information, equation (16) assumes an upper limit for k_d equal to k_{21}.

5. Determining S_f(IS) and α(IS)

[23] The above information indicates that colloid transport and retention will be very sensitive to $\Phi_{min}(C_{is})$ because of its influence on S_f and α. Colloid transport and retention data under various IS conditions [*Bradford and Kim*, 2012] will be analyzed below to infer information on the dependency of S_f and α on IS, and the macroscopic adhesive interaction. Specifically, we examine whether observed experimental trends are consistent with theoretical estimates based on the mean value of $\Phi_{min}(C_{is})$ obtained from DLVO theory and measured zeta potentials [*Bradford and Kim*, 2012]. The experimental values of S_f and α were obtained by simulating the measured breakthrough curves during phases 1 and 2 with the outlined model and simultaneously optimizing S_f and α to the data. The Pearson's correlation coefficient (R^2) between observed and simulated breakthrough curves during phases 1 and 2 was typically >0.92. However, the R^2 value for the 0.11 μm CML colloids at an IS = 106 mM was somewhat lower (0.57) because only 2.3% of the injected mass broke through in the column effluent.

[24] Figure 1 presents experimental and predicted values of S_f as a function of IS for 0.11 and 1.1 μm CML colloids during phases 1 and 2. The predicted values of S_f were obtained using equations (11) and (12) in conjunction with reported values of Φ_{min} [*Bradford and Kim*, 2012] and JKR theory [*Johnson et al.*, 1971] to determine $T_{adhesion}$. Experimental values of S_f shown in Figure 1 tended to gradually increase with IS, reflecting greater numbers of retention sites when the double layer thickness was compressed and Φ_{min} increased. These values of S_f were always low, but S_f was much higher for the 0.11 μm CML colloids ($S_f < 0.075$) than the 1.1 μm CML colloids ($S_f < 0.009$) at a given IS. This indicates that more retention sites were available for the smaller colloids. These same trends were observed for predicted values of S_f, but the difference with size was much larger than experimentally observed. DLVO calculations that were used to predict S_f reflect only the average adhesive interactions with the SWI (Φ_{min} and $T_{adhesion}$). To better understand the experimental and predicted values of S_f we need to consider the potentially significant influence of physical (e.g., surface roughness) and/or chemical (e.g., adsorbed multivalent cations) heterogeneity observed on the salt-treated sand [*Bradford and Kim*, 2012]. Surface integration techniques have been developed and utilized to calculate colloid interaction energies on idealized, microscopically heterogeneous solid surfaces [*Hoek and Agarwal*, 2006; *Duffadar and Davis*, 2007]. Surface integration calculations indicate that the strength of the interaction energy will vary spatially on the SWI, and that local minima in the interaction energy that are favorable for attachment may occur near heterogeneities [*Duffadar and Davis*, 2008]. The area of the zone of electrostatic influence is proportional to the colloid radius size and inversely related to the Debye-Huckel parameter [*Duffadar and Davis*, 2008]. A greater portion of the zone of electrostatic influence will therefore be occupied by a given sized heterogeneity for smaller colloids and higher IS. Consequently, smaller colloids and higher IS are associated with more locations on a

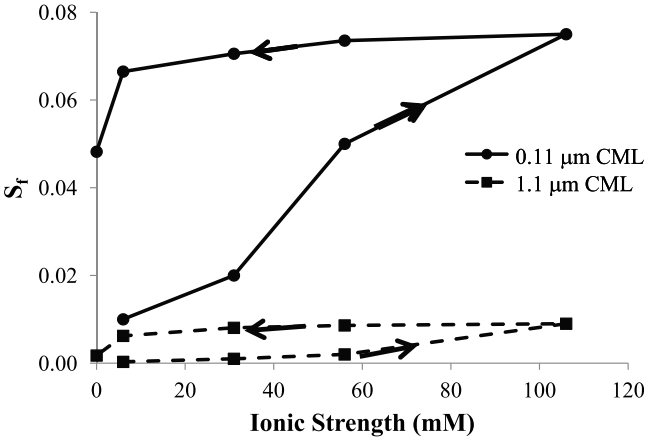

Figure 2. Hysteretic values of S_f for 0.11 and 1.1 μm CML colloids when phases 1and 2 (arrow to the right) were conducted at IS = 106 mM and phase 3 (arrow to the left) consisted of step decreases in IS equal to 56, 31, 6, and 0 mM. Experimental values of S_f were obtained by optimization of the simulated and measured breakthrough curves during phases 1 and 2, whereas equation (17) was used to predict S_f during phase 3.

microscopically heterogeneous SWI that have primary minimum interactions that contribute to S_f.

[25] The predicted value of S_f will also depend on the local balance of $T_{applied}$ and $T_{adhesion}$ for unfavorable locations with a secondary minimum (equations (11) and (12)). Both $T_{applied}$ and $T_{adhesion}$ are functions of r_c, but $T_{applied}$ decreases more rapidly (proportional to r_c^3) than $T_{adhesion}$ with r_c. Hence, S_f was predicted to be larger for smaller r_c (Figure 1) even though Φ_{min} was also smaller. It should be mentioned that this same result will hold for unfavorable locations on a heterogeneous SWI. However, in this case the local value of Φ_{min} on unfavorable locations is expected to be much lower as a result of surface roughness [*Hoek and Agarwal*, 2006; *Bendersky and Davis*, 2011] and because the zeta potential is more negative than in favorable locations. Both of these factors will produce lower values of S_f on a heterogeneous than a comparable homogeneous, smooth SWI that was assumed in our DLVO calculations. Errors in the predicted values of S_f (especially for smaller colloids) therefore reflect the importance of microscopic heterogeneities on colloid immobilization, and the inability of mean zeta potentials to account for these observations.

[26] Recall that s_{max} and S_f are linearly related through equation (10) when retention locations are filled. Similarly, it is logical to expect a linear relationship between the equilibrium value of s (s_{eq}) at a new IS and S_f when retention locations are incompletely filled as (cf. equations (3), (4), and (15)):

$$s_{eq} = \frac{S_f}{S_{if}} s_i = f_c s_i \tag{17}$$

This equation was subsequently used to estimate values of S_f during phase 3. Values of s_i (model output) and S_{if} (Figure 1) used in this calculation were determined after completion of phases 1 and 2, and a mass balance was conducted for each step reduction in IS of phase 3 to determine s_{eq}.

[27] Figure 2 shows hysteretic values of S_f for 0.11 and 1.1 μm CML colloids as a function of IS. Values of S_f during phases 1 and 2 (arrow to the right) were taken from experimental values shown in Figure 1, whereas equation (17) was used to predict S_f during phase 3 (arrow to the left) as the IS was decreased from 106 to 56, 31, 6, and 0 mM. Hysteresis in S_f occurred for both 0.11 and 1.1 μm CML colloids, but was greater for the smaller colloids. DLVO calculations indicate that the secondary minimum decreases and the height of the energy barrier to the primary minimum increases as the IS decreases. Consequently, a reduction in solution IS tends to induce release of colloids from a secondary minimum, but not from a primary minimum. As mentioned above, more primary minima interactions are expected for smaller colloids on a heterogeneous SWI because a greater portion of the zone of electrostatic influence is occupied by a given sized heterogeneity [*Duffadar and Davis*, 2007, 2008]. Clearly, physical and/or chemical heterogeneity played a significant role in determining S_f for 0.11 μm CML colloids

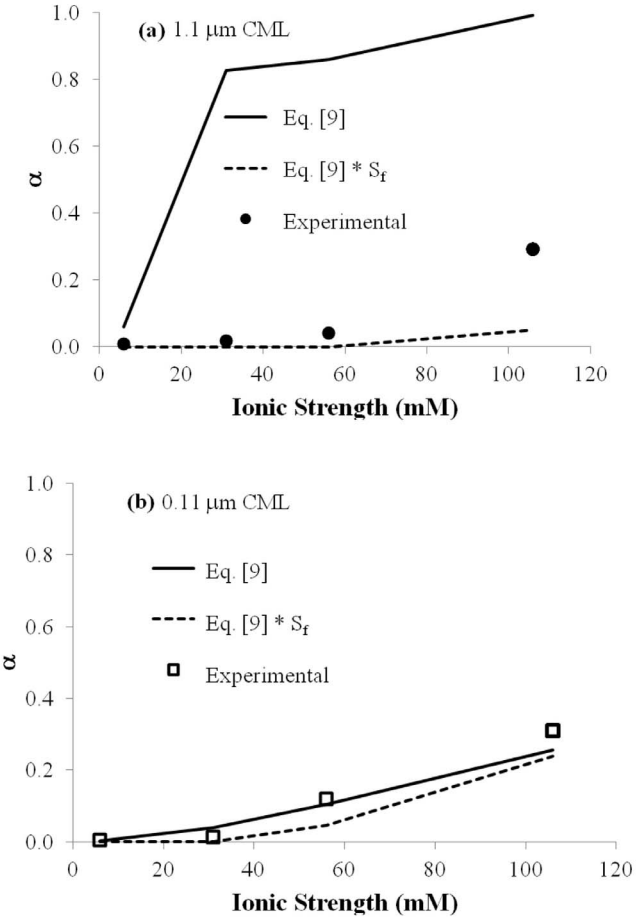

Figure 3. Experimental and predicted values of α as a function of IS for (a) 1.1 and (b) 0.11 μm CML microspheres. Experimental values of α were obtained by optimization of the simulated and measured breakthrough curves during phases 1 and 2. The predicted values of α were initially obtained from Φ_{min} [*Bradford and Kim*, 2012] using equation (9). This prediction was subsequently corrected for the influence of velocity by multiplying equation (9) by S_f (obtained from predictions shown in Figure 1).

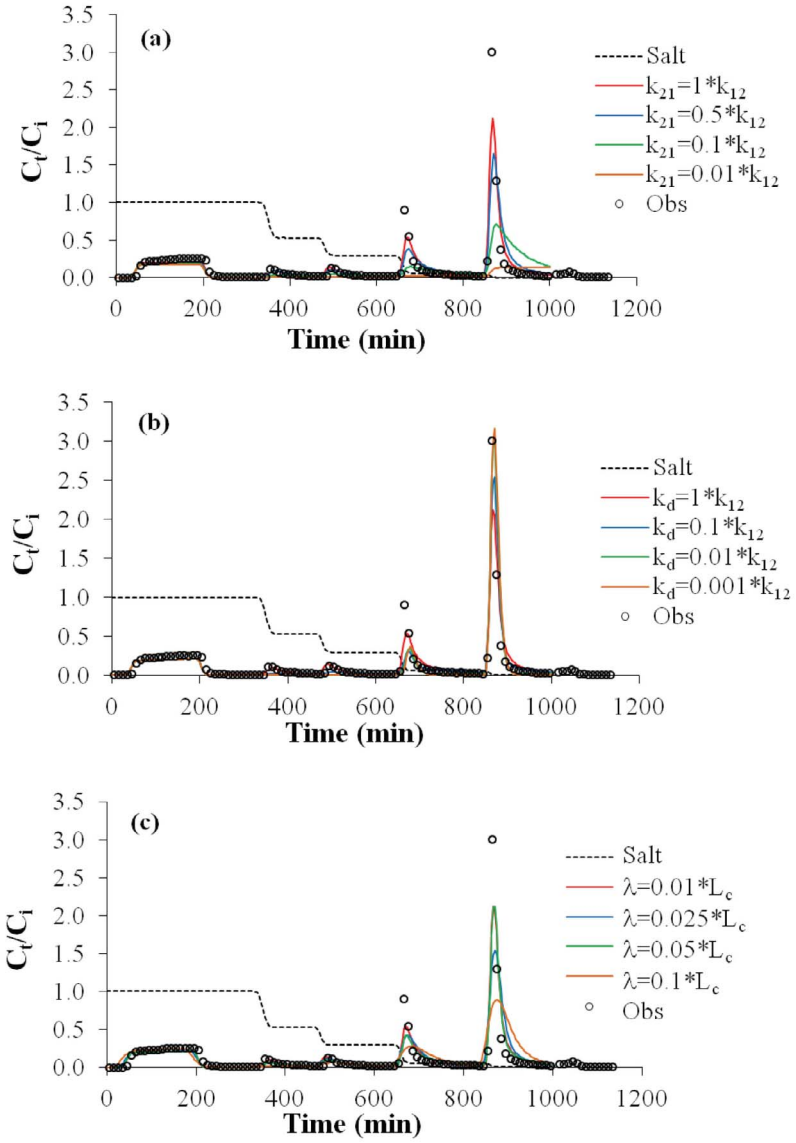

Figure 4. Observed and simulated transport and release behavior for 1.1 μm CML colloids when phases 1 and 2 were conducted at IS = 106 mM and phase 3 consisted of step decreases in IS equal to 56, 31, 6, and 0 mM. The values of (a) k_{21}, (b) k_d, and (c) λ are systematically varied. Other model parameters are given in Table 1.

and the interaction was therefore largely irreversible (primary minimum). In contrast, 1.1 μm CML colloids experienced a largely reversible interaction with less hysteresis, suggesting that the heterogeneity was sufficiently small relative to the zone of electrostatic influence to create a secondary minimum interaction.

[28] Figure 3 presents experimental and predicted values of α as a function of IS for 0.11 (Figure 3a) and 1.1 (Figure 3b) μm CML colloids. Initial estimates of α at different IS were obtained from Φ_{min} using equation (9). Experimental and predicted (equation (9)) values of α both increased with IS, reflecting greater amounts of retention when the double layer thickness was compressed and Φ_{min} increased. Furthermore, experimental and predicted (equation (9)) values of α were similar in magnitude at a given IS for the 0.11 μm CML colloids (Figure 3a). In contrast, predicted values of α were much larger than experimental values for the 1.1 μm CML colloids (Figure 3b). One potential explanation is due to hydrodynamic forces. Experimental values of α have been reported to decrease with increasing water velocity [*Johnson et al.*, 2007; *Shen et al.*, 2010]. *Shen et al.* [2010] accounted for this velocity dependency by multiplying α (equation (9)) by S_f (equations (11) and (12)). Predicted values of αS_f shown in Figure 3b were in closer agreement with experimental values of α then predictions based only on equation (9). However, this approach does not account for solid phase mass transfer from unfavorable to favorable regions. Consequently, the predicted velocity dependency of α is expected to be overestimated, especially for larger colloids. Indeed, predicted values of αS_f underestimated the experimental value of α for the 1.1 μm CML colloids at higher IS (Figure 3b).

[29] Piecewise cubic interpolation functions for S_f(IS) and α(IS) were used in subsequent simulations based on

Table 1. Model Parameters Used in Simulations Shown in Figures 4 and 5

Parameter	Values Used in Simulations
θ_{wt}	0.32 to 0.36
q_t	0.09 to 0.12 cm min^{-1}
L_c	11 to 13 cm
λ	(0.018 to 0.0025)*L_c, except for Figure 4c
d_{50}	360 μm
θ_{w1}, θ_{w2}, q_1, q_2	*Bradford et al.* [2011b]
k_{12}	*Yao et al.* [1971] and *Tufenkji and Elimelech* [2004]
k_{21}	k_{12}, except for Figure 4a
k_{2s}	Equation (13)
N_f	N_f = 5 for Figures 4, 5a, 5c, and 5d; equation (14) was used in Figure 5b with d_f = 1 μm
k_d	Equation (16), except Figure 4b
α(IS)	Interpolation function of fitted values of α during phases 1 and 2
S_f(IS)	Equation (17) using measured values of s_{eq} and fitted S_{if} during phases 1 and 2
s_i	Model output after completion of phases 1 and 2
f_c	Equation (15)
$s_{\max}$	Equation (10)
Colloid diameter	0.11 and 1.1 μm for CML, 0.5 μm for *E. coli* D21g,[a] and 0.027 μm for φX174
Pulse duration	160 min for CML, 75 min for *E. coli* D21g, and 70 min for φX174

[a]Selected to be consistent with the width of *E. coli* D21g.

experimental information similar to that shown in Figures 1 and 3, respectively.

6. Sensitivity Analysis

[30] In this section we investigate the sensitivity of colloid release with transient in IS to the parameters k_{21}, k_d, and λ. Figure 4 presents observed and simulated transport and release behavior for 1.1 μm CML colloids when phases 1 and 2 were conducted at IS = 106 mM, and phase 3 consisted of step decreases in IS equal to 56, 31, 6, and 0 mM. All concentrations are normalized by the maximum input concentration (C_i). The values of k_{21}, k_d, and λ are systematically varied, as indicated in the legends of Figures 4a, 4b, and 4c, respectively. Other model parameters are given in Table 1. Notice that release during phase 3 is sensitive to the values of k_{21}, k_d, and λ. In particular, higher values of k_{21} and k_d are required to accurately capture observed release behavior. High values of k_{21} and k_d imply that release during phase 3 is not consistent with a slow diffusion controlled processes as is commonly assumed, but is rather controlled by system hydrodynamics and changes in the torque balance with IS. However, it should be noted that colloid release is much lower in phase 2 than 3 due to a lower value of k_d = 0 and C_2, and a higher value of α that yields lower $(1 - \alpha)k_{21}$. Results from solute transport studies in columns indicate that the value of λ is typically around 0.1*L_c [*Vanderborght and*

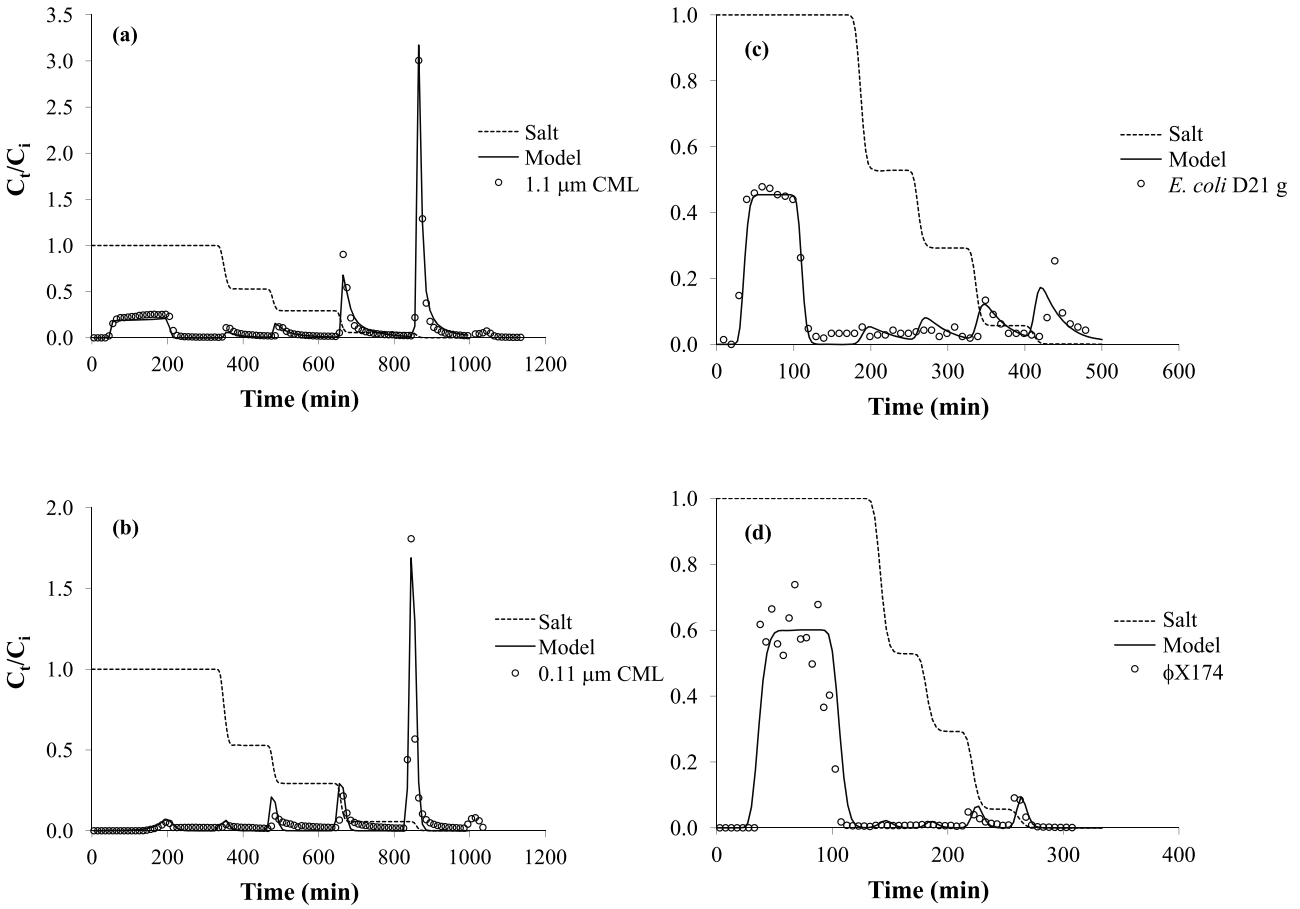

Figure 5. Observed and simulated transport and release for 1.1 and 0.11 μm CML microspheres, *E. coli* D21g, and φX174. Simulation parameters are summarized in Table 1.

Vereecken, 2007]. However, considerably lower values of λ were required to capture the observed trends for colloid release during phase 3. One plausible explanation is due to explicitly accounting for differences in the velocity in regions 1 and 2 of our dual-permeability model formulation.

7. Simulation of Experimental Data

[31] Figure 5 presents representative observed and simulated transport and release for 1.1 and 0.11 μm CML microspheres, *E. coli* D21g, and φX174. Simulation parameters were predicted from measured data (α(IS) and S_f(IS)), or selected based on the results of the sensitivity analyses discussed above. Table 1 provides a summary of the simulation parameters. The agreement between observed and simulated behavior is quite good (the mean square error <0.008 and the R^2 ranged from 0.80 to 0.98), indicating that the model formulation provided a satisfactory description of a variety of colloid release data with transients in IS. It should be mentioned that the above model formulation effectively lumps first-order microbial death and inactivation into the retention term for simplicity. Death and inactivation terms could have been explicitly added to the model formulation if desired, but were not needed because little death/inactivation occurred during these relatively short duration experiments [*Bradford and Kim*, 2012]. *Bradford and Kim* [2012] discuss in detail the differences in the release behavior for 1.1 and 0.11 μm CML microspheres, *E. coli* D21g, and φX174. In brief, these differences are mainly due to the hysteretic dependency of S_f on IS shown in Figure 2. In particular, the value of S_f determines the amount of release with transients in IS by directly influencing f_c according to equation (15).

8. Conclusions

[32] A sophisticated dual-permeability model was extended to simulate colloid transport and release with transients in solution IS by inclusion of a detachment term that is dependent on torque balance information (equations (3), (4), and (15)–(17)), and by making α and S_f functions of IS. This model was subsequently used to analyze experimental transport and release data with transients in IS for two sized latex microspheres, *E. coli* D21g, and coliphage φX174. Comparison of experimental and predicted values of α suggested that hydrodynamic forces likely influenced α, especially for larger colloids. Experimental values of S_f with IS were found to be consistent with expected trends on microscopically heterogeneous surfaces, and exhibited hysteresis with transients in IS. Greater hysteresis in S_f with IS occurred for smaller colloids likely because they are similar in size to microscale heterogeneities and exhibited more irreversible primary minimum interactions. Release of colloids during transient IS conditions were consistent with the modeled balance of applied hydrodynamic and resisting adhesive torques under unfavorable attachment conditions. Colloid release rates were shown to be very high (not diffusion controlled) once torque balance criteria for release were satisfied. All of this information improves our understanding and ability to simulate colloid release with transients in IS, and highlights the need to account for hysteretic adhesive interactions on microscopically heterogeneous surfaces. Results strongly indicate that additional research is needed to better predict α and S_f as a function of IS on heterogeneous surfaces and at different velocities.

[33] **Acknowledgments.** We would like to thank Lorena Altamirano for her help in conducting the transport experiments. This research was supported by the ARS, USDA, NP 214. The USDA is an equal opportunity provider and employer.

References

Adamczyk, Z., B. Siwek, M. Zembala, and P. Belouschek (1994), Kinetics of localized adsorption of colloid particles, *Adv. Colloid Interface Sci.*, *48*, 151–280.

Bales, R. C., S. R. Hinkle, T. W. Kroeger, K. Stocking, and C. P. Gerba (1991), Bacteriophage adsorption during transport through porous media: Chemical perturbations and reversibility, *Environ. Sci. Technol.*, *25*, 2088–2095.

Bendersky, M., and J. M. Davis (2011), DLVO interaction of colloidal particles with topographically and chemically heterogeneous surfaces, *J. Colloid Interface Sci.*, *353*, 87–97.

Bergendahl, J., and D. Grasso (1998), Colloid generation during batch leaching tests: Mechanics of disaggregation, *Colloids Surf. A*, *135*, 193–205.

Bergendahl, J., and D. Grasso (1999), Prediction of colloid detachment in a model porous media: Thermodynamics, *AIChE J.*, *45*, 475–484.

Bergendahl, J., and D. Grasso (2000), Prediction of colloid detachment in a model porous media: Hydrodynamics, *Chem. Eng. Sci.*, *55*, 1523–1532.

Bradford, S. A., and H. Kim (2010), Implications of cation exchange on clay release and colloid-facilitated transport in porous media, *J. Environ. Qual.*, *39*, 2040–2046.

Bradford, S. A., and H. Kim (2012), Causes and implications of colloid and microorganisms retention hysteresis, *J. Contam. Hydrol.*, *138-139*, 83–92, doi:10.1016/j.jconhyd.2012.06.007.

Bradford, S. A., S. Torkzaban, and S. L. Walker (2007), Coupling of physical and chemical mechanisms of colloid straining in saturated porous media, *Water Res.*, *41*, 3012–3024.

Bradford, S. A., H. Kim, B. Z. Haznedaroglu, S. Torkzaban, and S. L. Walker (2009), Coupled factors influencing concentration-dependent colloid transport and retention in saturated porous media, *Environ. Sci. Technol.*, *43*, 6996–7002.

Bradford, S. A., S. Torkzaban, and A. Wiegmann (2011a), Pore-scale simulations to determine the applied hydrodynamic torque and colloid immobilization, *Vadose Zone J.*, *10*, 252–261.

Bradford, S. A., S. Torkzaban, and J. Simunek (2011b), Modeling colloid transport and retention in saturated porous media under unfavorable attachment conditions, *Water Resour. Res.*, *47*, W10503, doi:10.1029/2011WR010812.

Derjaguin, B. V., and L. D. Landau (1941), Theory of the stability of strongly charged lyophobic sols and of the adhesion of strongly charged particles in solutions of electrolytes, *Acta Physicochim. URSS*, *14*, 733–762.

Derjaguin, B. V., V. M. Muller, and Y. P. Toporov (1975), Effect of contact deformations on the adhesion of particles, *J. Colloid Interface Sci.*, *53*, 314–326.

Dong, H., T. C. Onstott, C.-H. Ko, A. D. Hollingsworth, D. G. Brown, and B. J. Mailloux (2002), Theoretical prediction of collision efficiency between adhesion-deficient bacteria and sediment grain surface, *Colloids Surf. B*, *24*, 229–245.

Duffadar, R. D., and J. M. Davis (2007), Interaction of micrometer-scale particles with nanotextured surfaces in shear flow, *J. Colloid Interface Sci.*, *308*, 20–29.

Duffadar, R. D., and J. M. Davis (2008), Dynamic adhesion behavior of micrometer-scale particles flowing over patchy surfaces with nanoscale electrostatic heterogeneity, *J. Colloid Interface Sci.*, *326*, 18–27.

Foppen, J. W. A., and J. F. Schijven (2006), Evaluation of data from the literature on the transport and survival of *Escherichia coli* and thermotolerant coliforms in aquifers under saturated conditions, *Water Res.*, *40*, 401–426.

Gargiulo, G., S. A. Bradford, J. Simunek, P. Ustohal, H. Vereecken, and E. Klumpp (2007), Bacteria transport and deposition under unsaturated conditions: The role of the matrix grain size and the bacteria surface protein, *J. Contam. Hydrol.*, *92*, 255–273.

Gargiulo, G., S. A. Bradford, J. Simunek, P. Ustohal, H. Vereecken, and E. Klumpp (2008), Bacteria transport and deposition under unsaturated

flow conditions: The role of water content and bacteria surface hydrophobicity, *Vadose Zone J.*, *7*, 406–419.

Gmeiner, J., and S. Schlecht (1980), Molecular composition of the outer membrane of *Escherichia coli* and the importance of protein-lipopolysaccharide interactions, *Arch. Microbiol.*, *127*, 81–86.

Goldshmid, J., D. Zohar, Y. Argamon, and Y. Kott (1973), *Effects of Dissolved Salts on the Filtration of Coliform Bacteria in Sand Dunes*, Pergamon, New York.

Grolimund, D., and M. Borkovec (2006), Release of colloidal particles in natural porous media by monovalent and divalent cations, *J. Contam. Hydrol.*, *87*, 155–175.

Grolimund, D., K. Barmettler, and M. Borkovec (2001), Release and transport of colloidal particles in natural porous media: 2. Experimental results and effects of ligands, *Water Resour. Res.*, *37*, 571–582.

Hoek, E. M. V., and G. K. Agarwal (2006), Extended DLVO interactions between spherical particles and rough surfaces, *J. Colloid Interface Sci.*, *298*, 50–58.

Hubbe, M. A. (1984), Theory of detachment of colloidal particles from flat surfaces exposed to flow, *Colloids Surf.*, *12*, 151–178.

Israelachvili, J. N. (1992), *Intermolecular and Surface Forces*, Academic, San Diego, Calif.

Johnson, K. L., K. Kendall, and A. D. Roberts (1971), Surface energy and the contact of elastic solids, *Proc. R. Soc. London, Ser. A*, *324*, 301–313.

Johnson, P. R., and M. Elimelech (1995), Dynamics of colloid deposition in porous media: Blocking based on random sequential adsorption, *Langmuir*, *11*, 801–812.

Johnson, W. P., X. Li, and S. Assemi (2007), Deposition and re-entrainment dynamics of microbes and non-biological colloids during non-perturbed transport in porous media in the presence of an energy barrier to deposition, *Adv. Water Resour.*, *30*, 1432–1454.

Khilar, K. C., and H. S. Fogler (1984), The existence of a critical salt concentration for particle release, *J. Colloid Interface Sci.*, *101*, 214–224.

Kim, H. N., S. A. Bradford, and S. L. Walker (2009), *Escherichia coli* O157:H7 transport in saturated porous media: Role of solution chemistry and surface macromolecules, *Environ. Sci. Technol.*, *43*, 4340–4347.

Kim, S.-B., S.-J. Park, C.-G. Lee, and H.-C. Kim (2008), Transport and retention of *Escherichia coli* in a mixture of quartz, Al-coated and Fe-coated sands, *Hydrol. Processes*, *22*, 3856–3863.

Lenhart, J. J., and J. E. Saiers (2003), Colloid mobilization in water-saturated porous media under transient chemical conditions, *Environ. Sci. Technol.*, *37*, 2780–2787.

Li, X., P. Zhang, C. L. Lin, and W. P. Johnson (2005), Role of hydrodynamic drag on microsphere deposition and re-entrainment in porous media under unfavorable conditions, *Environ. Sci. Technol.*, *39*, 4012–4020.

Maugis, D. (1992), Adhesion of spheres: The JKR-DMT transition using a dugdale model, *J. Colloid Interface Sci.*, *150*, 243–269.

McDowell-Boyer, L. M. (1992), Chemical mobilization of micron-sized particles in saturated porous media under steady flow conditions, *Environ. Sci. Technol.*, *26*, 586–593.

Metge, D. W., R. W. Harvey, G. R. Aiken, R. Anders, G. Lincoln, and J. Jasperse (2010), Influence of organic carbon loading, sediment associated metal oxide content and sediment grain size distributions upon *Cryptosporidium parvum* removal during riverbank filtration operations, Sonoma County, CA, *Water Res.*, *44*, 1126–1137.

Nocito-Gobel, J., and J. E. Tobiason (1996), Effects of ionic strength on colloid deposition and release, *Colloids Surf. A*, *107*, 223–231.

Roy, S. B., and D. A. Dzombak (1996), Colloid release and transport processes in natural and model porous media, *Colloids Surf. A*, *107*, 245–262.

Ryan, J. N., and M. Elimelech (1996), Colloid mobilization and transport in groundwater, *Colloids Surf. A*, *107*, 1–56.

Ryan, J. N., and P. M. Gschwend (1994), Effects of ionic-strength and flow-rate on colloid release: Relating kinetics to intersurface potential-energy, *J. Colloid Interface Sci.*, *164*, 21–34.

Sharma, M. M., H. Chamoun, D. S. H. S. R. Sarma, and R. S. Schechter (1992), Factors controlling the hydrodynamic detachment of particles from surfaces, *J. Colloid Interface Sci.*, *149*, 121–134.

Shen, C., B. Li, Y. Huang, and Y. Jin (2007), Kinetics of coupled primary- and secondary-minimum deposition of colloids under unfavorable chemical conditions, *Environ. Sci. Technol.*, *41*, 6976–6982.

Shen, C., Y. Huang, B. Li, and Y. Jin (2010), Predicting attachment efficiency of colloid deposition under unfavorable attachment conditions, *Water Resour. Res.*, *46*, W11526, doi:10.1029/2010WR009218.

Shiratori, K., Y. Yamashita, and Y. Adachi (2007), Deposition and subsequent release of Na-kaolinite particles by adjusting pH in the column packed with Toyoura sand, *Colloids Surf. A*, *306*, 137–141.

Simoni, S. F., H. Harms, T. N. P. Bosma, and A. J. B. Zehnder (1998), Population heterogeneity affects transport of bacteria through sand columns at low flow rates, *Environ. Sci. Technol.*, *32*, 2100–2105.

Torkzaban, S., S. A. Bradford, and S. L. Walker (2007), Resolving the coupled effects of hydrodynamics and DLVO forces on colloid attachment to porous media, *Langmuir*, *23*, 9652–9660.

Torkzaban, S., S. S. Tazehkand, S. L. Walker, and S. A. Bradford (2008), Transport and fate of bacteria in porous media: Coupled effects of chemical conditions and pore space geometry, *Water Resour. Res.*, *44*, W04403, doi:10.1029/2007WR006541.

Torkzaban, S., S. L. Walker, and S. A. Bradford (2009), Reply to comment by William P. Johnson et al. on "Transport and fate of bacteria in porous media: Coupled effects of chemical conditions and pore space geometry," *Water Resour. Res.*, *45*, W09604, doi:10.1029/2008WR007576.

Torkzaban, S., H. N. Kim, J. Simunek, and S. A. Bradford (2010), Hysteresis of colloid retention and release in saturated porous media during transients in solution chemistry, *Environ. Sci. Technol.*, *44*, 1662–1669.

Tosco, T., A. Tiraferri, and R. Sethi (2009), Ionic strength dependent transport of microparticles in saturated porous media: Modeling mobilization and immobilization phenomena under transient chemical conditions, *Environ. Sci. Technol.*, *43*, 4425–4431.

Tsai, C.-J., D. Y. H. Pui, and B. Y. H. Liu (1991), Particle detachment from disk surfaces of computer disk drives, *J. Aerosol Sci.*, *22*, 737–746.

Tufenkji, N., and M. Elimelech (2004), Correlation equation for predicting single-collector efficiency in physicochemical filtration in saturated porous media, *Environ. Sci. Technol.*, *38*, 529–536.

Vanderborght, J., and H. Vereecken (2007), Review of dispersivities for transport modeling in soils, *Vadose Zone J.*, *6*, 29–52.

Verwey, E. J. W., and J. T. G. Overbeek (1948), *Theory of the Stability of Lyophobic Colloids*, Elsevier, Amsterdam.

Walker, S. L., J. A. Redman, and M. Elimelech (2004), Role of cell surface lipopolysaccharides in *Escherichia coli* K12 adhesion and transport, *Langmuir*, *20*, 7736–7746.

Wang, D., M. Paradelo, S. A. Bradford, W. J. G. M. Peijnenburg, L. Chu, and D. Zhou (2011), Facilitated transport of Cu with hydroxyapatite nanoparticles in saturated sand: Effects of solution ionic strength and composition, *Water Res.*, *45*, 5905–5915.

Yao, K.-M., M. T. Habibian, and C. R. O'Melia (1971), Water and waste water filtration: Concepts and applications, *Environ. Sci. Technol.*, *5*, 1105–1112.